

Comparing fermionic superfluids in two and three dimensions

Lennart Sobirey,^{1,*} Hauke Biss,^{1,2} Niclas Luick,^{1,2} Markus Bohlen,^{1,2} Henning Moritz,^{1,2} and Thomas Lompe^{1,2}

¹*Institut für Laserphysik, Universität Hamburg*

²*The Hamburg Centre for Ultrafast Imaging, Universität Hamburg, Luruper Chaussee 149, 22761 Hamburg*

(Dated: June 23, 2021)

Understanding the origins of unconventional superconductivity has been a major focus of condensed matter physics for many decades. While many questions remain unanswered, experiments have found that the systems with the highest critical temperatures tend to be layered materials where superconductivity occurs in two-dimensional (2D) structures [1–3]. However, to what extent the remarkable stability of these strongly correlated 2D superfluids is related to their reduced dimensionality is still an open question [3]. In this work, we use dilute gases of ultracold fermionic atoms [4, 5] as a model system to directly observe the influence of dimensionality on strongly interacting fermionic superfluids. We achieve this by measuring the superfluid gap of a strongly correlated quasi-2D Fermi gas [6, 7] over a wide range of interaction strengths and comparing the results to recent measurements in 3D Fermi gases [8]. We find that the superfluid gap follows the same universal function of the interaction strength in both systems, which suggests that there is no inherent difference in the stability of fermionic superfluidity between two- and three-dimensional quantum gases. Finally, we compare our data to results from solid state systems and find a similar relation between the interaction strength and the gap for a wide range of two- and three-dimensional superconductors.

Fermionic particles such as the electrons in superconductors have half-integer spin and therefore obey the Pauli exclusion principle. This prevents systems of non-interacting fermions from condensing into a macroscopic wavefunction and becoming superfluid. However, in the presence of an effective attractive interaction it can become energetically favorable for fermions with opposite spin to form bosonic pairs. These pairs can then condense into a coherent many-body state and become superfluid, as laid out by Bardeen, Cooper and Schrieffer (BCS) in their famous theory of superconductivity [9]. The energy that is required to break one of these pairs is called the superfluid gap Δ , as the pairing manifests itself as a gap in the excitation spectrum of fermionic superfluids. Since breaking the pairs destroys the superfluid, the size of this

gap determines the stability of the superfluid and sets its critical temperature.

Over the last decades, new classes of superconductors have been discovered that exhibit higher critical temperatures and stronger interactions than conventional BCS superconductors [10]. Of particular interest are systems where superfluidity occurs in two-dimensional structures, as they are the ones where the highest ambient-pressure critical temperatures have been observed [1]. However, the dimensionality of these systems cannot be changed without dramatically altering their other properties as well, and it is therefore unclear to what extent the surprising stability of their superfluidity is predicated on their two-dimensional nature.

In this work, we directly observe the effect of reduced dimensionality on the stability of strongly interacting fermionic superfluids. We measure the superfluid gap of an ultracold 2D Fermi gas as a function of interaction strength and compare the results with our recent measurement of the gap in a three-dimensional system [8]. We find that the superfluid gap follows the same universal function of the chemical potential in both systems, which suggests that dimensionality has only limited influence on the stability of strongly interacting fermionic superfluids.

For our experiments, we use ultracold atomic Fermi gases of ⁶Li atoms. Such gases have two key advantages that make them uniquely suited for performing experiments that isolate the effect of dimensionality on the stability of superfluids: The first is that they are systems with simple and well-understood interparticle interactions that can be easily tuned using Feshbach resonances [12]. The second is that the dimensionality of the system can be controlled freely by changing the shape of the confining potential [13–20]. By combining these two features, we can create two- and three-dimensional systems that have the same microscopic physics but different dimensionality.

To perform a quantitative comparison between these systems, we examine the effect of the reduced dimensionality on the superfluid gap. The gap is well suited for this purpose, as it directly determines both the critical current and the critical temperature of a fermionic superfluid and thus constitutes an excellent measure for its stability. As reliable measurements of the gap are available for three-dimensional Fermi gases [8, 21, 22], we can focus our experiments on measuring the gap in two-dimensional systems.

* lsobirey@physnet.uni-hamburg.de

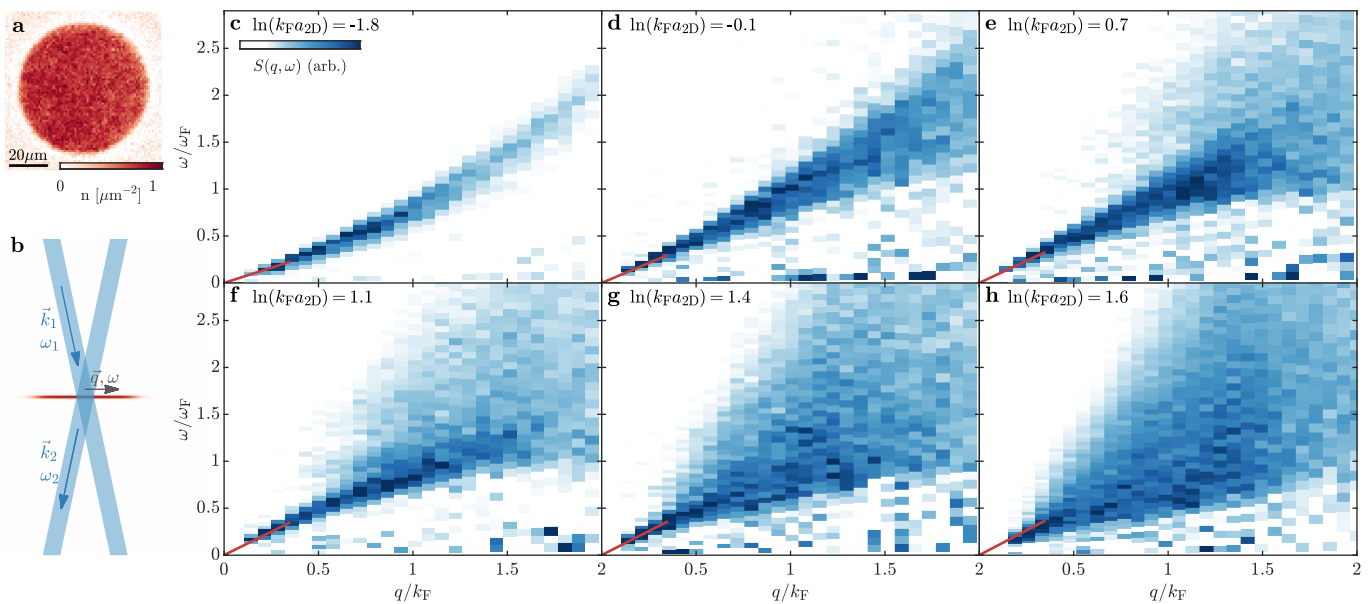


FIG. 1. **Excitation spectrum of a 2D Fermi gas in the BEC-BCS crossover.** **a:** Absorption image showing the density $n(\vec{r})$ of our homogeneous 2D Fermi gas. **b:** Sketch of the experimental setup for measuring the excitation spectrum of our system. Two far-detuned laser beams drive a two-photon transition with energy and momentum transfer $\hbar\omega = \hbar(\omega_1 - \omega_2)$ and $\hbar q = \hbar|\vec{k}_1 - \vec{k}_2|$, and the dynamic structure factor $S(q, \omega)$ can be obtained from the resulting heating rate. **c-h:** Measurements of $S(q, \omega)$ taken at different values of the 2D interaction parameter $\ln(k_F a_{2D})$. For strong attractive interactions (**c**), the system consists of tightly bound molecules which are excited as unbroken pairs, and consequently $S(q, \omega)$ shows the Bogoliubov dispersion of an interacting Bose gas. Moving into the crossover regime (**d, e, f**), the pairs become more weakly bound and pair breaking excitations begin to appear at higher momenta. These excitations become more pronounced as we approach the BCS limit where the system shows the expected broad pair breaking continuum (**g, h**). In addition to these pair breaking excitations, it is also possible to excite sound waves in the superfluid. These appear in our spectra as a linear mode at low momenta, with a slope that corresponds to the speed of sound in the system and is in excellent agreement with previous measurements (red lines in panels **c-h**, [11]). The data in panel **a** (**c-h**) was obtained by averaging over 26 (3-8) individual measurements. The behavior observed in (**c-h**) closely resembles results obtained in 3D Fermi gases [8] (for a comparison see Supplementary Materials).

To bring our system into the two-dimensional regime, we apply a strong confining potential along one direction such that the chemical potential and temperature are well below the level spacing. This strongly suppresses all excitations in this direction and thereby creates an effective (or quasi-) 2D system [6, 7, 23] (see Supplementary Materials).

We then measure the excitation spectrum of the gas to determine the size of the superfluid gap. We use momentum resolved Bragg spectroscopy to measure the dynamic structure factor $S(q, \omega)$ of the superfluid, which describes the probability of creating an excitation in the system by providing an energy and momentum transfer of $\hbar\omega$ and $\hbar q$ (Fig. 1**b**, see Supplementary Materials). By tuning the strength of the interparticle interactions, we can perform such measurements throughout the crossover from a BCS superfluid of weakly bound Cooper pairs to a Bose-Einstein-condensate (BEC) of deeply bound molecules, where the interaction strength can be parametrized by the 2D interaction parameter $\ln(k_F a_{2D})$. Here, a_{2D} is the 2D scattering length [23], $k_F = \sqrt{2mE_F}/\hbar$ is the Fermi

wavevector, $E_F = \hbar\omega_F$ is the Fermi energy, and m is the mass of a ${}^6\text{Li}$ atom.

The results of these measurements are shown in Fig. 1**c-h**. We observe two different types of excitations [24]: The first are longer-range collective excitations of the superfluid, which are visible as a linear sound mode at low momentum transfers ($q \ll k_F$), with a slope that is in excellent agreement with the speed of sound measured in [11] (red lines in Fig. 1**c-h**). This is the Goldstone mode of the system, which arises from the breaking of the U(1) symmetry of the system when the gas condenses into a superfluid [22, 25]. The second type of excitations are single-particle excitations that break a pair. As this process is only possible if the energy transfer is sufficiently high to overcome the energy gained from pairing, these excitations show a sharp onset at an energy transfer of 2Δ . This behavior is most apparent for BCS superfluids with weak attractive interactions (Fig. 1**g, h**), where a pronounced continuum of pair breaking excitations is clearly visible. When increasing the interparticle attraction, the size of the su-

perfluid gap increases and consequently the onset of the pair breaking continuum shifts towards higher energies. Additionally, as the pairs are transformed from weakly bound Cooper pairs to tightly bound bosonic molecules, the onset of the pair breaking continuum moves towards higher momenta as pair breaking excitations are suppressed when the size of the pairs becomes small compared to the length scale of the perturbation [26, 27]. This trend continues into the BEC regime, where the molecules are so tightly bound that pair breaking excitations become completely suppressed. The excitation spectrum then exhibits the well-known Bogoliubov dispersion relation of a superfluid Bose gas, which consists of a linear dispersion of phonons at low momentum and single-particle excitations of bosonic molecules at higher momenta (see Fig. 1 c).

To determine the superfluid gap Δ from our measurements, we integrate the measured dynamic structure factors over the momentum axis. The resulting quantity $S(\omega) = \int S(q, \omega) q dq$ describes the probability of creating an excitation with a given energy $\hbar\omega$ and is similar to the Raman response measured in inelastic Raman scattering experiments in solid state physics [31]. On the BCS side of the crossover, our measurements of $S(\omega)$ show the same behavior as observed in the Raman response of s-wave BCS superconductors: A sharp increase at 2Δ , followed by a slow decay back to zero [32] (Fig. 2a). In the BCS regime, we can therefore directly extract the size of the superfluid gap from $S(\omega)$ (see Supplementary Materials).

Towards the BEC regime, extracting quantitative information from $S(\omega)$ becomes more difficult as the onset of the pair breaking continuum is masked by an increasing weight of the Goldstone mode. Fortunately, we can circumvent this problem by probing the system at lower momenta, where the energy of phononic excitations is significantly below 2Δ [8, 22]. While pair breaking excitations are suppressed at these low wavevectors, they can still be observed when using a stronger drive. This is shown in Fig. 2b, where the onset of the pair breaking mode at 2Δ is clearly separated from the strongly driven Goldstone mode visible at lower energy. Employing both of these methods enables us to measure the superfluid gap Δ throughout the BEC-BCS crossover. The resulting values are plotted as a function of the 2D interaction parameter $\ln(k_F a_{2D})$ in Fig. 2c, together with the binding energy E_B of the bare two-body bound state (red line), which in 2D systems exists for any non-zero attractive interaction [6]. For our smaller attractive interactions ($\ln(k_F a_{2D}) \gtrsim 1.5$), the two-body binding energy is negligible, and the sizable gap of $\Delta \approx 0.3 E_F$ is entirely due to many-body effects. However, when going into the crossover regime, the trivial two-body binding energy increases and becomes comparable to the effect of the many-body BCS pairing. To separate these two contributions to the gap and thereby determine the

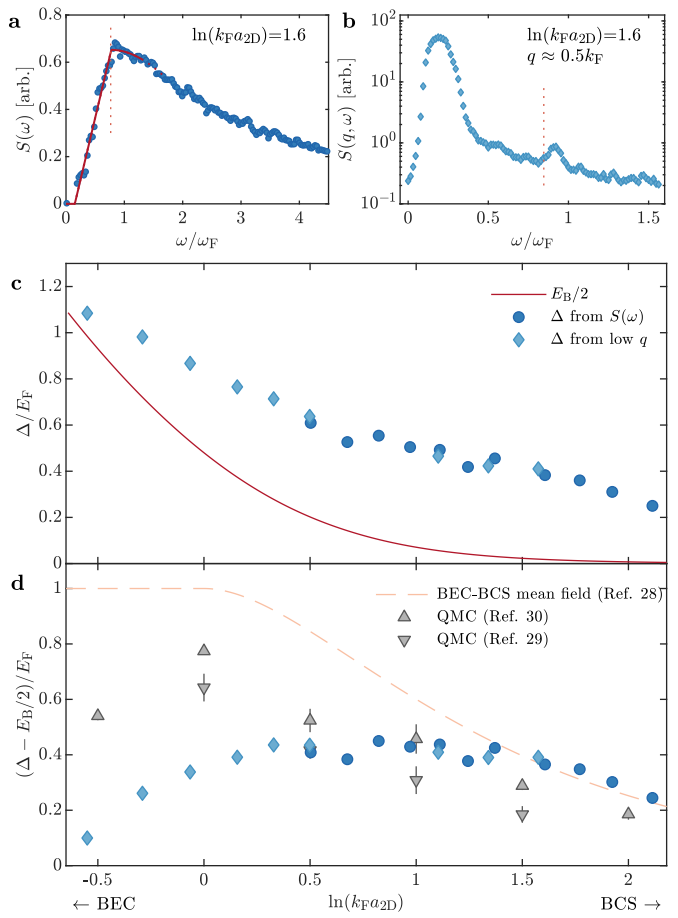


FIG. 2. Superfluid gap in the 2D BEC-BCS crossover.

a: Integrated dynamic structure factor $S(\omega) = \int S(q, \omega) q dq$ at an interaction strength of $\ln(k_F a_{2D}) = 1.6$. We determine the energy 2Δ (red dotted line) at which pair breaking excitations become possible from a phenomenological fit (solid red line) to $S(\omega)$ (see Supplementary Materials). **b:** Dynamic structure factor $S(q, \omega)$ measured at a fixed momentum transfer of $q = 0.5 k_F$. At these small wavevectors, pair breaking is suppressed and strong driving is required to observe the onset of the pair breaking mode at 2Δ (red dotted line), which causes a strong saturation of the low-energy phononic mode. **c:** Measured superfluid gap Δ as a function of the interaction strength. The different symbols distinguish results obtained using the approaches shown in panel **a** ($S(\omega)$, blue dots) and **b** (low q , light blue diamonds). The contribution of the two-body bound state to the gap is shown as a dark red line. **d:** Many-body contribution $\Delta - E_B/2$ to the superfluid gap Δ . BEC-BCS mean field predictions (dashed orange line, [28]) are in agreement with our measurement in the BCS regime, but deviate in the strongly correlated crossover regime. Quantum Monte-Carlo calculations (gray triangles, [29, 30]) show better agreement in the crossover, but still deviate from the measurements in the BEC regime. Error bars denote 1σ confidence intervals of the fit and are smaller than the symbol size, the data shown in panels **a** (**b**) is the average of 8 (26) individual measurements.

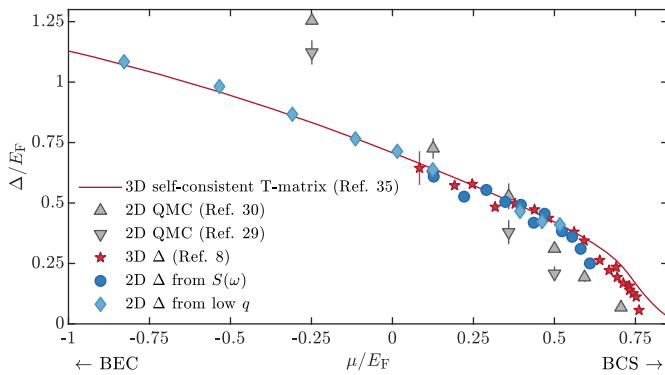


FIG. 3. Comparing the gap of two-dimensional and three-dimensional superfluids. Superfluid gap Δ/E_F of two-dimensional (blue circles and diamonds) and three-dimensional (red stars) Fermi gases as a function of the chemical potential μ/E_F , for which we use the results of QMC calculations [33, 34]. The measurements of the gap collapse onto a single curve, which is well-described by theoretical predictions for the gap in three-dimensional Fermi gases (red line [35, 36]); results from 2D QMC calculations [29, 30] are shown as gray diamonds (see Supplementary Materials). Error bars denote 1σ confidence intervals of the fit.

evolution of the many-body contribution throughout the crossover, we subtract the known value of the two-body binding energy [6] from our measured gaps. As can be seen in Fig. 2d, the many-body contribution $\Delta - E_B/2$ grows with increasing interactions in the BCS regime, reaches a maximum in the crossover regime and then decreases again towards the BEC side of the resonance, where the contribution of the two-body bound state begins to dominate as the gas turns into a BEC of deeply bound molecules. When comparing these results to theory, we find that they are in excellent agreement with mean-field theory [28] in the BCS regime, but begin to deviate from the mean-field results in the strongly correlated crossover region ($\ln(k_F a_{2D}) \approx 1$). Quantum Monte-Carlo (QMC) simulations [29, 30] are in somewhat better agreement with our data in the crossover, but still predict larger values of $\Delta - E_B/2$ in the BEC regime.

We now proceed to compare our measurements to recent results from 3D Fermi gases. To perform such a comparison, we need to find a suitable parametrization of the interaction strength, as the dimensionless interaction parameters $\ln(k_F a_{2D})$ and $1/k_F a_{3D}$ that are commonly used in two- and three-dimensional systems parametrize the interactions differently and cannot be compared directly. Instead, we parametrize the interaction strength with the normalized chemical potential μ/E_F of the fermions. This choice is motivated by the fact that the chemical potential is a basic thermodynamic quantity that is defined independent of dimensionality and has monotonous and well-known relations to the 2D and 3D interaction parameters $\ln(k_F a_{2D})$ and $1/k_F a_{3D}$ [33, 34, 38, 39]. Therefore,

we can perform our comparison by plotting the superfluid gap Δ/E_F as a function of the chemical potential μ/E_F for two- and three-dimensional systems. The results are shown in Fig. 3.

Remarkably, we find that within the accuracy of our measurements, the results for Δ/E_F obtained in two- and three-dimensional systems collapse onto a single curve. This suggests that for strongly interacting Fermi gases, the gap follows a single, universal function $f(\mu/E_F) = \Delta/E_F$ of the interaction strength that is independent of the dimensionality of the system. The data appears to be well-described by theoretical predictions for three-dimensional fermionic superfluids [35], but as shown in Fig. 2d deviates from 2D QMC calculations [29, 30]. This is unlikely to be the result of imperfect two-dimensional confinement or thermal excitations, which would both be expected to have the strongest effect in the BCS regime (see Supplementary Materials). Consequently, our measurements imply that for a given coupling strength, there is no inherent difference in the stability of fermionic superfluidity between two- and three-dimensional quantum gases.

As we perform our experiments in an ideal model system, it is natural to ask to what extent our results apply to other, more complex materials. The first step to answering this question is to extend Fig. 3 by adding data from other fermionic superfluids. However, while the chemical potential provides an excellent measure for the interaction strength in our strongly interacting quantum gases, there is a large number of materials where it is not known with sufficient accuracy to be used as a parametrization of the interaction strength. We therefore need a different interaction parameter that is viable in a wide variety of systems including ultracold gases, liquid ^3He and solid state superconductors. One parameter that has been suggested for this purpose is the dimensionless pair size ξk_F [28, 40–43]. Similar to the chemical potential, ξk_F describes a fundamental physical property whose definition is independent of the dimensionality of the system. Additionally, ξ is closely related to the coherence length [44], which has been measured in many solid state superconductors.

To obtain an estimate of the pair size for our systems, we consider the momentum dependence of the pair breaking excitations observed in our measurements of the dynamic structure factor in two- and three-dimensional Fermi gases [8]. As discussed above, these measurements show a suppression of pair breaking excitations when the wavelength of the probing lattice becomes comparable to the size of the pairs. We can therefore fit the onset of the pair breaking continuum on the momentum axis and relate the onset momentum $\hbar k_o$ to the pair size via $k_o \sim 1/\xi$, with a prefactor that can be determined by comparing the results to theoretical predictions for two-dimensional [45] and three-dimensional [46] systems (see Supplementary Materials). We plot the resulting values

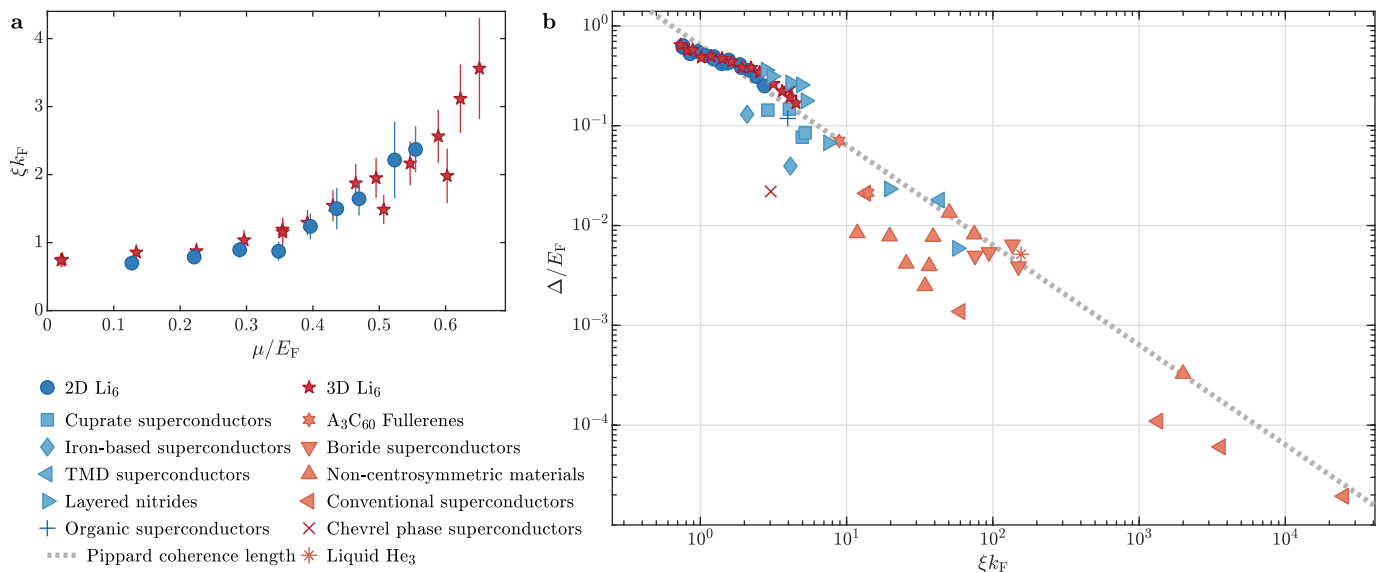


FIG. 4. **Fermionic superfluidity in different materials.** **a:** Dimensionless pair size ξk_F plotted as a function of the dimensionless chemical potential μ/E_F . As ξk_F follows the same function of μ/E_F for the two- and three-dimensional systems, ξk_F can be used as an alternative parametrization of the interaction strength in our strongly interacting Fermi gases. Error bars denote 1σ confidence intervals. **b:** Plot of the dimensionless gap Δ/E_F against the dimensionless pair size ξk_F for different fermionic superfluids. The Pippard coherence length $\xi_p = \frac{\hbar^2 k_F}{\pi m \Delta}$ [37] is shown as a dotted line. Remarkably, the superfluid gap is roughly proportional to the inverse of the dimensionless pair size for a wide range of materials which span five orders of magnitude in Δ/E_F and ξk_F . This observation applies equally to two- and three-dimensional systems, which suggests that strong correlations are more important for the stability of fermionic superfluids than the dimensionality of the system.

of ξk_F as a function of μ/E_F and find that the results for the two- and three-dimensional systems collapse onto a single curve (Fig. 4a). This shows that our estimate of ξk_F can be used as an alternate parametrization of the interaction strength in ultracold Fermi gases [43].

Consequently, we can now plot our measurements of the gap Δ/E_F as a function of the pair size ξk_F and compare the results to a wide variety of different superconductors. The results are shown in Fig. 4b. Remarkably, all materials fall into a single band, which extends from conventional superconductors with gaps on the order of $10^{-5} E_F$ and large coherence lengths to ultracold Fermi gases with gaps comparable to the Fermi energy and coherence lengths approaching the interparticle spacing, with a wide variety of exotic superconductors in between. Fig. 4b therefore clearly shows a direct correlation between shorter coherence lengths and larger gaps [10, 40] that holds from the weak coupling limit all the way into the strongly correlated regime. This correlation exists independent of the dimensionality of the material, in excellent agreement with our observations in two- and three-dimensional Fermi gases. Therefore, our findings suggest that there is no inherent increase in the stability of a fermionic superfluid in two dimensions compared to a three-dimensional system with the same coupling strength.

In this work, we have used measurements of the exci-

tation spectrum of strongly interacting ultracold Fermi gases to determine the superfluid gap and found that the gap follows a universal function of the interaction strength that is independent of the dimensionality. By extending the comparison to other fermionic superfluids, we have shown that this observation appears to hold for a wide range of two- and three-dimensional systems. Consequently, our results suggest that there is no inherent increase in the stability of the superfluid phase in lower dimensions.

Our work highlights that ultracold gases and strongly correlated superconductors can be realized at comparable effective interaction strengths. In particular, the range of interaction strengths accessible with ultracold Fermi gases has significant overlap with the tuning range of the coupling strength of recently realized two-dimensional materials such as magic-angle twisted trilayer graphene [47] and lithium-intercalated layered nitrides [48]. This raises the prospect of preparing ultracold gases and solid state systems that have the same effective interaction strength and directly comparing their properties. For example, this could enable comparative studies of the transition from a superfluid to a strongly correlated normal state, which in 2D quantum gases has been observed to also show strong many-body pairing [49] and is difficult to study in many solid state systems due to the presence of competing order parameters [1, 50–52].

We thank G. Salomon, J. P. Brantut and L. Mathey for helpful comments on the manuscript. This work is supported by the Deutsche Forschungsgemeinschaft (DFG, German Research Foundation) in the framework of SFB-925 – project 170620586 - and the excellence cluster 'Advanced Imaging of Matter' - EXC 2056 - project 390715994.

-
- [1] B. Keimer, S. A. Kivelson, M. R. Norman, S. Uchida, and J. Zaanen, *Nature* **518**, 179 (2015).
- [2] J.-F. Ge, Z.-L. Liu, C. Liu, C.-L. Gao, D. Qian, Q.-K. Xue, Y. Liu, and J.-F. Jia, *Nat. Mater.* **14**, 285 (2015).
- [3] Y. Yu, L. Ma, P. Cai, R. Zhong, C. Ye, J. Shen, G. D. Gu, X. H. Chen, and Y. Zhang, *Nature* **575**, 156 (2019).
- [4] I. Bloch, J. Dalibard, and W. Zwerger, *Rev. Mod. Phys.* **80**, 885 (2008).
- [5] W. Ketterle and M. W. Zwierlein, in *Proceedings of the International School of Physics-Enrico Fermi*, edited by M Inguscio, S Stringari, (2008).
- [6] J. Levinsen and M. M. Parish, in *Annual Review of Cold Atoms and Molecules*, Annual Review of Cold Atoms and Molecules, Vol. 3 (WORLD SCIENTIFIC, 2015) pp. 1–75.
- [7] A. V. Turlapov and M. Yu Kagan, *J. Phys. Condens. Matter* **29**, 383004 (2017).
- [8] H. Biss, L. Sobirey, N. Luick, M. Bohlen, J. J. Kinnunen, G. M. Bruun, T. Lompe, and H. Moritz, (2021), arXiv:2105.09820 [cond-mat.quant-gas].
- [9] J. Bardeen, L. N. Cooper, and J. R. Schrieffer, *Physical review* **108**, 1175 (1957).
- [10] Y. J. Uemura, L. P. Le, G. M. Luke, B. J. Sternlieb, W. D. Wu, J. H. Brewer, T. M. Riseman, C. L. Seaman, M. B. Maple, M. Ishikawa, D. G. Hinks, J. D. Jorgensen, G. Saito, and H. Yamochi, *Phys. Rev. Lett.* **66**, 2665 (1991).
- [11] M. Bohlen, L. Sobirey, N. Luick, H. Biss, T. Enss, T. Lompe, and H. Moritz, *Phys. Rev. Lett.* **124**, 240403 (2020).
- [12] C. Chin, R. Grimm, P. Julienne, and E. Tiesinga, *Rev. Mod. Phys.* **82**, 1225 (2010).
- [13] K. Martiyanov, V. Makhalov, and A. Turlapov, *Phys. Rev. Lett.* **105**, 030404 (2010).
- [14] B. Fröhlich, M. Feld, E. Vogt, M. Koschorreck, W. Zwerger, and M. Köhl, *Phys. Rev. Lett.* **106** (2011).
- [15] A. T. Sommer, L. W. Cheuk, M. J. H. Ku, W. S. Bakr, and M. W. Zwierlein, *Phys. Rev. Lett.* **108**, 045302 (2012).
- [16] M. G. Ries, A. N. Wenz, G. Zürn, L. Bayha, I. Boettcher, D. Kedar, P. A. Murthy, M. Neidig, T. Lompe, and S. Jochim, *Phys. Rev. Lett.* **114**, 230401 (2015).
- [17] C. Cheng, J. Kangara, I. Arakelyan, and J. E. Thomas, *Phys. Rev. A* **94**, 031606 (2016).
- [18] D. Mitra, P. T. Brown, P. Schauß, S. S. Kondov, and W. S. Bakr, *Phys. Rev. Lett.* **117**, 093601 (2016).
- [19] T. Peppler, P. Dyke, M. Zamorano, I. Herrera, S. Hoinka, and C. J. Vale, *Phys. Rev. Lett.* **121**, 120402 (2018).
- [20] K. Hueck, N. Luick, L. Sobirey, J. Siegl, T. Lompe, and H. Moritz, *Phys. Rev. Lett.* **120**, 060402 (2018).
- [21] A. Schirotzek, Y.-I. Shin, C. H. Schunck, and W. Ketterle, *Phys. Rev. Lett.* **101**, 140403 (2008).
- [22] S. Hoinka, P. Dyke, M. G. Lingham, J. J. Kinnunen, G. M. Bruun, and C. J. Vale, *Nat. Phys.* **13**, 943 (2017).
- [23] D. S. Petrov and G. V. Shlyapnikov, *Phys. Rev. A* **64**, 012706 (2001).
- [24] While in principle a third type of excitations exists in the form of the Higgs mode, this mode is expected to lie within the pair breaking continuum [53]) and is therefore not visible in our spectra.
- [25] J. Goldstone, *Il Nuovo Cimento* (1955-1965) **19**, 154 (1961).
- [26] A. J. Leggett, *J. Phys. Chem. Solids* **59**, 1729 (1998).
- [27] H. P. Büchler, P. Zoller, and W. Zwerger, *Phys. Rev. Lett.* **93**, 080401 (2004).
- [28] M. Randeria, J. M. Duan, and L. Y. Shieh, *Phys. Rev. Lett.* **62**, 981 (1989).
- [29] E. Vitali, H. Shi, M. Qin, and S. Zhang, *Phys. Rev. A* **96**, 061601 (2017).
- [30] T. Zielinski, B. Ross, and A. Gezerlis, *Phys. Rev. A* **101**, 033601 (2020).
- [31] T. P. Devereaux and R. Hackl, *Rev. Mod. Phys.* **79**, 175 (2007).
- [32] M. V. Klein and S. B. Dierker, *Phys. Rev. B Condens. Matter* **29**, 4976 (1984).
- [33] G. E. Astrakharchik, J. Boronat, J. Casulleras, Giorgini, and S, *Phys. Rev. Lett.* **93**, 200404 (2004).
- [34] H. Shi, S. Chiesa, and S. Zhang, *Phys. Rev. A* **92**, 033603 (2015).
- [35] R. Haussmann, W. Rantner, S. Cerrito, and W. Zwerger, *Phys. Rev. A* **75**, 023610 (2007).
- [36] Note that we plot the gap from [35] against the chemical potential from [33] instead of the value for μ/E_F obtained in [35]. However, as the two results for the chemical potential are very similar, this does not significantly affect the comparison or its conclusion.
- [37] N. W. Ashcroft and N. D. Mermin, *Solid state physics* (New York: Holt, Rinehart and Winston., 1976).
- [38] I. Boettcher, L. Bayha, D. Kedar, P. A. Murthy, M. Neidig, M. G. Ries, A. N. Wenz, G. Zürn, S. Jochim, and T. Enss, *Phys. Rev. Lett.* **116**, 045303 (2016).
- [39] M. J. H. Ku, A. T. Sommer, L. W. Cheuk, and M. W. Zwierlein, *Science* **335**, 563 (2012).
- [40] F. Pistolesi and G. C. Strinati, *Phys. Rev. B Condens. Matter* **49**, 6356 (1994).
- [41] S. Stintzing and W. Zwerger, *Phys. Rev. B Condens. Matter* **56**, 9004 (1997).
- [42] C. H. Schunck, Y.-I. Shin, A. Schirotzek, and W. Ketterle, *Nature* **454**, 739 (2008).
- [43] F. Marsiglio, P. Pieri, A. Perali, F. Palestini, and G. C. Strinati, *Phys. Rev. B Condens. Matter* **91**, 054509 (2015).
- [44] F. Pistolesi and G. C. Strinati, *Phys. Rev. B Condens. Matter* **53**, 15168 (1996).
- [45] M. Randeria, J. M. Duan, and L. Y. Shieh, *Phys. Rev. B Condens. Matter* **41**, 327 (1990).
- [46] M. Marini, F. Pistolesi, and G. C. Strinati, *Eur. Phys. J. B* **1**, 151 (1998).
- [47] J. M. Park, Y. Cao, K. Watanabe, T. Taniguchi, and P. Jarillo-Herrero, *Nature* **590**, 249 (2021).
- [48] Y. Nakagawa, Y. Kasahara, T. Nomoto, R. Arita, T. Nomura, and Y. Iwasa, *Science* **372**, 190 (2021).
- [49] P. A. Murthy, M. Neidig, R. Klemt, L. Bayha, I. Boettcher, T. Enss, M. Holten, G. Zürn, P. M. Preiss, and S. Jochim, *Science* **359**, 452 (2018).

- [50] T. Kondo, Y. Hamaya, A. D. Palczewski, T. Takeuchi, J. S. Wen, Z. J. Xu, G. Gu, J. Schmalian, and A. Kaminski, *Nat. Phys.* **7**, 21 (2011).
- [51] T. Kondo, A. D. Palczewski, Y. Hamaya, T. Takeuchi, J. S. Wen, Z. J. Xu, G. Gu, and A. Kaminski, *Phys. Rev. Lett.* **111**, 157003 (2013).
- [52] M. Hashimoto, I. M. Vishik, R.-H. He, T. P. Devereaux, and Z.-X. Shen, *Nat. Phys.* **10**, 483 (2014).
- [53] H. Zhao, X. Gao, W. Liang, P. Zou, and F. Yuan, *New J. Phys.* **22**, 093012 (2020).

SUPPLEMENTARY MATERIALS

Sample preparation and experimental procedure

For the preparation of our homogeneous 2D Fermi gases, we use the experimental setup and procedure described in [20, 54]. In brief, we use first laser- and then evaporative cooling to prepare ultracold gases of approximately 6000 fermionic ${}^6\text{Li}$ atoms in a balanced mixture of the two lowest-energy hyperfine states. In the radial direction, the gas is held in place by a repulsive ring potential with a diameter of about $70\ \mu\text{m}$, resulting in a density per spin state of $n = 0.8\ \text{atoms}/\mu\text{m}^2$, corresponding to $E_F \approx h \cdot 8.5\ \text{kHz}$. In the vertical direction, an optical lattice provides a tight harmonic confinement with a trapping frequency of $\hbar\omega_z = h \cdot 9.2\ \text{kHz}$. To control the interparticle interactions, we apply magnetic offset fields between 700 G and 1000 G. Due to the presence of a Feshbach resonance at a magnetic field of 832 G [55], this allows us to access interaction strengths throughout the BEC-BCS crossover. By ensuring that all interaction ramps are adiabatic, we keep the system at an approximately constant entropy per particle for all experiments. The entropy in our system corresponds to a temperature of $T = 0.04(1) T_F$ at an interaction strength of $\ln(k_F a_{2D}) = -2.9$, which according to [54] is well below the critical entropy for superfluidity in the crossover regime.

Influence of the third dimension

To obtain a quasi-2D system for our experiments, we trap our atoms in a highly anisotropic confinement, where the spacing of the energy levels in the tightly confined direction is much larger than the reduced chemical potential $\tilde{\mu} = \mu + E_B/2$ and the temperature T of the gas. In this regime, the interactions between the particles can be mapped onto an effective 2D interaction, and the long-range physics of the system become essentially two-dimensional [23]. However, on length scales that are comparable to the size of the tight confinement, there is still a residual influence from the third dimension that causes these short-range physics to be different from the ones found in a purely 2D system. Performing a quantitative comparison with purely 2D theories therefore requires taking into account these corrections. The most important difference compared to a purely 2D system is a modification of the two-body binding energy as discussed in [6], which for a quasi-2D geometry is given by

$$\frac{l_z}{a_{3D}} = \int_0^\infty \frac{du}{\sqrt{4\pi}u^3} \left(\frac{\exp(-\frac{E_B}{\hbar\omega_z}u)}{\sqrt{\frac{1}{2u}(1 - \exp(-2u))}} \right), \quad (\text{S1})$$

where l_z is the harmonic oscillator length of the tight harmonic confinement [6]. Equation S1 has been found to

be in good agreement with experiments, see e.g. [6, 49]. This modification of the binding energy is important when comparing our data to QMC results in Fig. 3, as these are obtained from purely 2D calculations. We therefore use the QMC results for the many-body contribution $\Delta - E_B/2$ and eq. S1 for the binding energy.

The influence of the third dimension also becomes relevant when there is a significant population of higher energy levels in the strongly confined direction. In our systems, the temperature is negligible compared to the level spacing ($T < 0.1 \hbar\omega_z$) [54], and we therefore neglect the influence of thermal excitations in the strongly confined direction. The second relevant quantity is the reduced chemical potential $\tilde{\mu}$. While $\tilde{\mu}$ increases towards the BCS regime [34], it remains well below the level spacing $\hbar\omega_z$ for our experiments. Nevertheless, for our larger values of $\tilde{\mu}/\hbar\omega_z$ there are modifications of the scattering physics of the system, which are taken into account in the definition of a_{2D} [7, 23].

Measuring the dynamic structure factor.

We obtain $S(q, \omega)$ by moving a weak Bragg lattice through the gas and measuring the resulting heating rate. The Bragg lattice is formed by two far-detuned laser beams focused onto the atoms with a high-resolution objective as described in [54]. Two acousto-optic modulators set the frequency difference of the two beams, while two motorized translation stages can be used to change their crossing angle. This enables us to perform two-photon spectroscopy of the gas with tunable energy and momentum transfer. To determine the heating rate caused by the Bragg lattice, we relate the decrease in the condensate fraction after an adiabatic interaction ramp to the BEC regime to the increase in the energy E of the system [54]. This in turn gives us access to the dynamic structure factor via the relation $S(q, \omega) \propto \frac{1}{\omega} \frac{dE}{dt}$ [56]. While thermal occupation of excitations can modify the measured spectrum [57], these effects are negligible for the low temperatures and comparatively high energy transfers in our experiments. We note that the increased noise in the measured dynamic structure factors at low frequencies is an artifact of the division by ω and does not suggest the presence of actual excitations in the system.

Chemical potential and binding energy

To plot our data as a function of the chemical potential in Fig. 3 and Fig. 4a, we need to perform a conversion between the 2D and 3D interaction parameters and the chemical potential. For the 3D data, we use the results of fixed-node diffusion Monte Carlo calculations performed in [33], which have been shown to be in good agreement with measurements of the equation of state in 3D Fermi

gases [39, 58]. For the 2D system, we use the auxiliary-field QMC calculations performed in [34], which are in good agreement with recent measurements [11, 38, 59]. We can therefore determine the chemical potential for our quasi-2D system by taking these results and including the appropriate binding energy given by eq. S1.

Determination of the superfluid gap.

To determine the size of the superfluid gap from our measurements of the dynamic structure factor, we employ two different methods. The first is based on taking measurements of $S(q, \omega)$ as shown in Fig. 1 and integrating over the momentum axis to obtain $S(\omega)$. While the exact line shape of $S(\omega)$ is unknown, we expect it to be qualitatively similar to the one observed in the Raman response of s-wave BCS superconductors, which exhibits a sharp onset at an energy of 2Δ followed by a slow decay. However, the presence of the Goldstone mode in neutral superfluids and additional effects such as Fourier broadening and density inhomogeneities modify the line shape and lead to nonzero values of $S(\omega)$ below 2Δ . We therefore fit our measurements of $S(\omega)$ with a phenomenological line shape consisting of a linear increase followed by a Gaussian decay, where the intersection point of the two parts is identified as 2Δ . The second method is based on the work performed in [22]. It relies on measuring $S(q, \omega)$ at a fixed momentum transfer q that is chosen such that the pair breaking mode is well separated from the low-energy Goldstone mode. This allows us to perform a simple bilinear fit to determine the onset of the pair breaking feature (see Fig. 2b), with the intersection point identified as 2Δ . Note that for large regions of the interaction strength we employ both methods to measure the superfluid gap and find very similar results.

Pair size determination

As stated in the main text, the pair size ξ can serve as an interaction parameter that is independent of the dimensionality of the system [40, 43] and is known for a large number of solid-state superfluids (see Table S1). However, for ultracold gases there is only a single study of the pair size in a 3D Fermi gas [42], and no pair size measurements have been performed in 2D Fermi gases at all. Therefore, we make use of the momentum dependence of pair breaking excitations to obtain an estimate for the pair size ξ from our measurements of the dynamic structure factor $S(q, \omega)$. In particular, we consider the suppression of pair breaking excitations that occurs when the wavelength $\lambda_0 = 2\pi/q$ of the probing lattice becomes comparable to the size of the pairs. This suppression can be understood by considering the differential force that acts on the constituents of a pair: If the

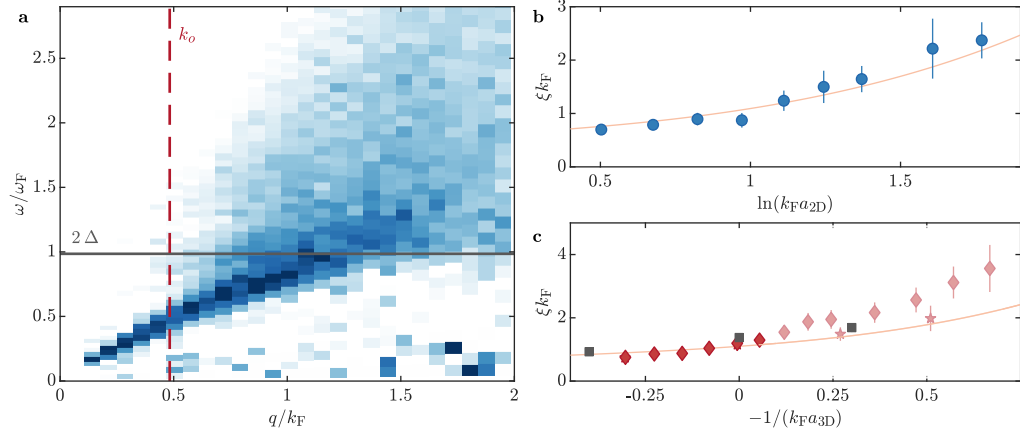
wavelength of the Bragg lattice is much larger than the pair size, the differential force vanishes and pair breaking becomes strongly suppressed. Consequently, the onset of the pair breaking continuum in the momentum axis is directly related to the size of the fermion pairs.

For our estimate of the pair size, we make the simple approximation that we can define an onset momentum k_o that is related to the pair size via $k_o = \alpha/\xi$ with a proportionality factor α . We identify k_o as the intersection point of a bilinear fit which is performed on a slice through the dynamic structure factor at a transferred energy of $\hbar\omega = 2\Delta$ (see Fig. S1a). To estimate the value of α , we compare our results for $1/k_o$ to theoretical predictions of ξ for the given dimensionality.

Fig. S1b shows the theoretical prediction for the pair size of a 2D Fermi gas from mean-field theory [45] together with our estimate of ξ , with a prefactor of $\alpha_{2D} \approx 0.6$. We find that the interaction dependence of our estimate is in excellent agreement with the mean-field prediction.

The comparison between the prediction for the pair size of a 3D Fermi gas from ref. [46] and our estimate of ξ using a prefactor of $\alpha_{3D} \approx 0.8$ is shown in Fig. S1c. As the determination of k_o becomes increasingly difficult towards the BCS regime where k_o approaches the smallest transferred momenta we can realize in our experimental setup, only measurements for $1/k_{Fa_{3D}} > -0.1$ were considered in the determination of α . In this interaction range, the interaction dependence of our estimate of ξ is then in good agreement with the theoretical prediction.

In addition, our estimate of ξ in 3D is in excellent agreement with the measurements of the pair size of a 3D Fermi gas performed in [42] using RF spectroscopy (black squares in Fig. S1c). This excellent agreement, as well as the very similar values of α for the 2D and 3D systems, strongly support the validity of our approach to determine ξ from our measurements of the dynamic structure factor. Additionally, we note that small changes in our estimate of ξ do not significantly affect the conclusions drawn from Fig. 4b.



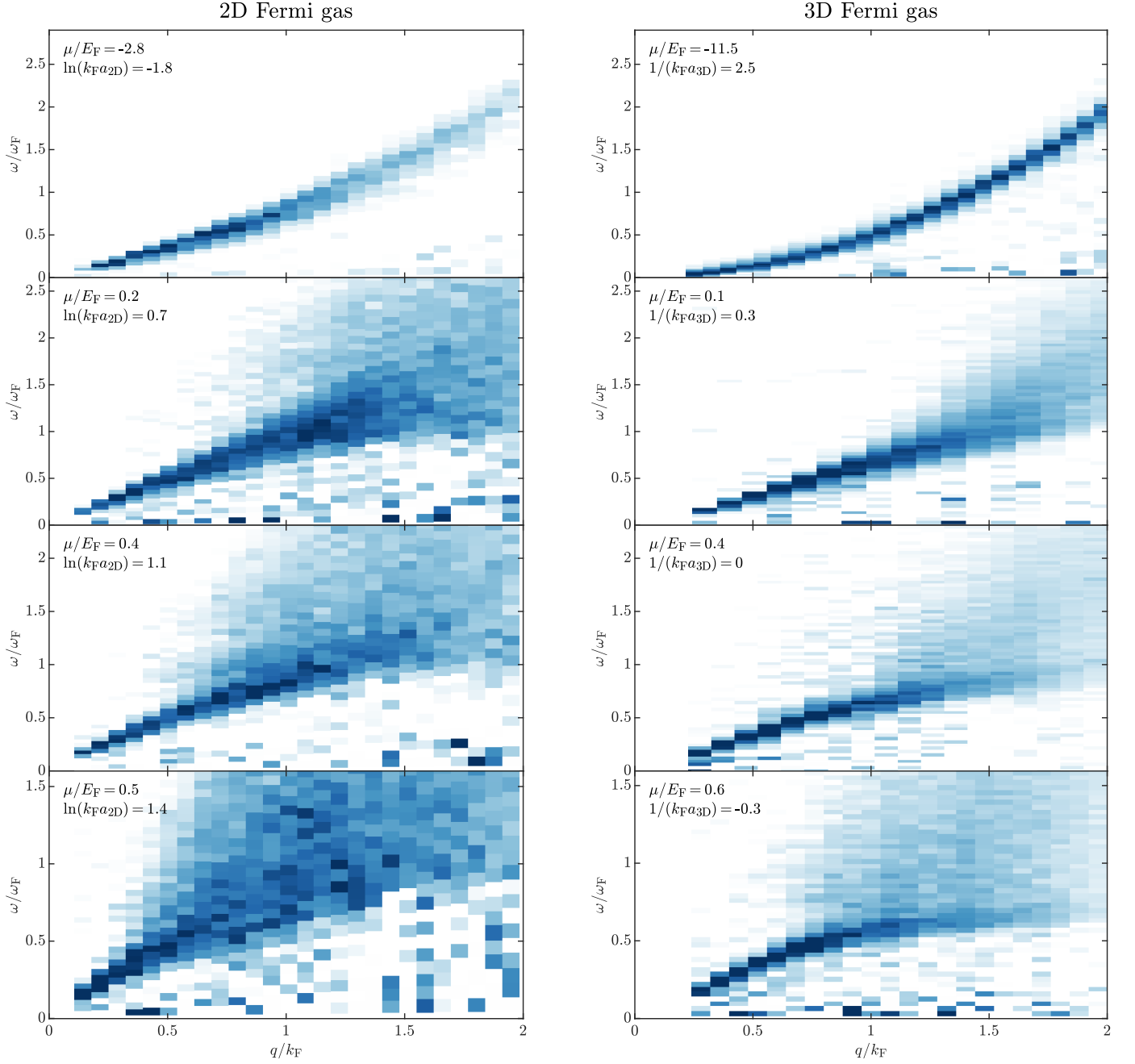
Supplementary Fig. S1. **Pair size in the BEC-BCS crossover** **a**: Estimation of the pair size from a measurement of the dynamic structure factor. We determine the onset momentum k_o (red-dashed vertical line) of the pair breaking continuum via a bilinear fit of the dynamic structure factor $S(q, 2\Delta)$ at a transferred energy of $\hbar\omega = 2\Delta$ (black horizontal line). We then obtain an estimate of the pair size $\xi \approx \alpha_{3D}/k_o$. **b**: Estimate of the pair size $\xi = \alpha_{2D}/k_o$ for a 2D Fermi gas (blue circles). The value of $\alpha_{2D} \approx 0.6$ is obtained by matching our results for k_o to the theoretical prediction [45] (solid line). **c**: Pair size $\xi = \alpha_{3D}/k_o$ for a 3D Fermi gas. Red stars denote data points where k_o was extracted from full measurements of the 3D structure factor as shown in **a**, red diamonds denote data from a separate set of measurements where data was only taken at transferred energies of $\hbar\omega \approx 2\Delta$. The solid line denotes a theory prediction from ref. [46], gray squares show results from a pair size measurement performed in ref. [42], rescaled as discussed in ref. [60]. Error bars denote 1σ confidence intervals of the fit.

Material	Δ/k_B [K]	E_F/k_B [K]	ξ [Å]	k_F [Å ⁻¹]	Ref.
Bi ₂ Sr ₂ CaCu ₂ O ₈	140	970	7.0	0.41	[61, 62]
Tl ₂ Ba ₂ Ca ₂ Cu ₃ O ₁₀	270	1800	7.3	0.49	[61, 63, 64]
La _{1.85} Sr _{0.15} CuO ₄	84	1100	11	0.46	[61, 62]
YBa ₂ Cu ₃ O ₇	470	8800	15	0.45	[61, 65, 66]
RbCa ₂ Fe ₄ As ₄ F ₂	95	730	10	0.20	[67]
FeSe/STO	240	6200	6.7	0.61	[2, 68]
Pb	13	120000	830	1.6	[69]
Sn	6.6	110000	2300	1.6	[69]
Al	2.1	110000	16000	1.6	[69]
Nb	18	13000	111	0.54	[48, 70, 71]
BaKBiO ₃	61	2900	53	0.26	[69, 72]
κ -(ET) ₂ Cu(NCS) ₂	25	210	23	0.17	[61, 73]
NbSe ₂	15	810	80	0.54	[74, 75]
PbMo ₆ S ₈	36	1600	9.8	0.31	[61, 76]
YB ₆	16	2400	330	0.41	[77]
YNi ₂ B ₂ C	21	4200	80	0.94	[77]
LuRuB ₂	16	4100	180	0.85	[78, 79]
YRuB ₂	13	2400	110	0.84	[78, 79]
K ₃ C ₆₀	33	470	26	0.34	[80, 81]
Rb ₃ C ₆₀	62	2900	29	0.49	[69, 81, 82]
Re ₃ Ta	8.6	640	110	0.46	[83]
Re _{5.5} Ta	16	2000	45	0.44	[84]
Nb _{0.5} Os _{0.5}	5.6	660	78	0.15	[85]
La ₇ Ir ₃	4.3	520	190	0.40	[86]
LaPtGe	4.9	1200	59	0.43	[87]
BeAu	5.8	18000	1900	1.1	[88]
TaOs	3.5	900	74	0.50	[89]
Zr ₃ Ir	4.1	1700	46	0.75	[90]
NbOs ₂	4.8	620	90	0.43	[91]
³ He	0.0046	0.89	200	0.78	[40, 92]
Li _x ZrNCl			tuneable		[48]

Supplementary Table S1. **Parameters for different fermionic superfluids in Fig. 4.** Values and references for the superconducting gap Δ , the Fermi energy E_F , the coherence length ξ and the Fermi wavevector k_F used in Fig. 4b. For materials such as cuprate superconductors where these parameters are dependent on the doping level, results for optimally doped samples were used. We note that there are different extrapolation methods and definitions of the coherence length, leading to different values between references. However, the differences are generally on the order of unity and therefore do not affect the conclusions drawn from Fig. 4b.

B [G]	$\ln(k_F a_{2D})$	Δ/E_F	μ/E_F	ξk_F	B [G]	$(k_F a_{3D})^{-1}$	Δ/E_F	μ/E_F	ξk_F
2D, Low q					3D, Low q				
784	-0.55	1.084(4)	-0.83	-	812	0.37	0.64(7)	0.08	0.73
792	-0.29	0.98(1)	-0.53	-	816	0.27	0.573(7)	0.19	0.82
800	-0.07	0.87(1)	-0.31	-	820	0.22	0.58(1)	0.27	0.89
808	0.16	0.77(1)	-0.11	-	824	0.15	0.48(2)	0.32	1.01
816	0.33	0.71(1)	0.01	0.70	828	0.08	0.497(7)	0.38	1.18
824	0.50	0.64(1)	0.12	0.76	832	0.01	0.47(1)	0.44	1.41
855	1.10	0.47(2)	0.39	1.23	835	-0.05	0.44(2)	0.48	1.63
871	1.34	0.423(6)	0.46	1.52	839	-0.12	0.384(5)	0.53	1.93
886	1.58	0.410(5)	0.52	1.86	843	-0.18	0.38(1)	0.56	2.22
2D, $S(\omega)$					847	-0.24	0.34(1)	0.59	2.54
824	0.50	0.61(1)	0.13	0.76	855	-0.35	0.26(1)	0.64	3.16
832	0.68	0.526(9)	0.22	0.85	3D, High q				
839	0.82	0.55(1)	0.29	0.96	863	-0.43	0.222(3)	0.67	3.63
847	0.97	0.50(1)	0.35	1.09	867	-0.51	0.24(2)	0.69	4.04
855	1.11	0.493(9)	0.40	1.24	871	-0.53	0.193(7)	0.69	4.11
863	1.24	0.42(1)	0.44	1.40	879	-0.62	0.1686(5)	0.71	4.51
871	1.37	0.46(1)	0.47	1.56	886	-0.73	0.16(1)	0.73	-
886	1.61	0.383(5)	0.52	1.91	886	-0.74	0.14(2)	0.73	-
898	1.77	0.360(8)	0.55	2.17	894	-0.83	0.126(2)	0.74	-
910	1.92	0.31(1)	0.58	2.42	902	-0.91	0.11(1)	0.75	-
926	2.11	0.25(2)	0.61	2.75	910	-0.98	0.057(7)	0.76	-

Supplementary Table S2. **Summary of experimental results.** Shown are the measured values of the gap for both 2D and 3D Fermi gases, with the values for the 3D Fermi gases taken from [8]. Also shown are the values of the chemical potential μ used in Fig. 3 (see Supplementary Materials) and the approximate value of ξk_F obtained from a spline fit to the data shown in Fig. 4a. Errors denote 1σ confidence intervals of the fit.



Supplementary Fig. S2. **Measurements of the dynamic structure factor in two- and three-dimensional ultracold Fermi gases.** The excitation spectra of systems with comparable values of μ/E_F show very similar qualitative behavior. 3D data taken from [8].

-
- [54] L. Sobirey, N. Luick, M. Bohlen, H. Biss, H. Moritz, and T. Lompe, *Science* **372**, 844 (2021).
- [55] G. Zürn, T. Lompe, A. N. Wenz, S. Jochim, P. S. Julienne, and J. M. Hutson, *Phys. Rev. Lett.* **110** (2013).
- [56] A. Brunello, F. Dalfovo, L. Pitaevskii, S. Stringari, and F. Zambelli, *Phys. Rev. A* **64**, 063614 (2001).
- [57] E. D. Kuhnle, S. Hoinka, P. Dyke, H. Hu, P. Hannaford, and C. J. Vale, *Phys. Rev. Lett.* **106**, 170402 (2011).
- [58] N. Navon, S. Nascimbène, F. Chevy, and C. Salomon, *Science* **328**, 729 (2010).
- [59] K. Fenech, P. Dyke, T. Peppler, M. G. Lingham, S. Hoinka, H. Hu, and C. J. Vale, *Phys. Rev. Lett.* **116**, 045302 (2016).
- [60] F. Palestini and G. C. Strinati, *Phys. Rev. B Condens. Matter* **89**, 224508 (2014).
- [61] D. R. Harshman and A. P. Mills, *Phys. Rev. B Condens. Matter* **45**, 10684 (1992).
- [62] T. Yoshida, M. Hashimoto, S. Ideta, A. Fujimori, K. Tanaka, N. Mannella, Z. Hussain, Z.-X. Shen, M. Kubota, K. Ono, and Others, *Phys. Rev. Lett.* **103**, 037004 (2009).
- [63] E. E. M. Chia, J.-X. Zhu, D. Talbayev, and A. J. Taylor, *Phys. Stat. Solidi. Rapid Res. Lett.* **5**, 1 (2011).
- [64] Y. G. Ponomarev, V. A. Alyoshin, E. V. Antipov, T. E. Oskina, A. Krapf, S. V. Kulbachinskii, M. G. Mikheev, M. V. Sudakova, S. N. Tchesnokov, and L. M. Fisher, *JETP Lett.* **100**, 126 (2014).
- [65] G. Grissonnanche, O. Cyr-Choinière, F. Laliberté, S. René de Cotret, A. Juneau-Fecteau, S. Dufour-Beauséjour, M.-È. Delage, D. LeBoeuf, J. Chang, B. J. Ramshaw, D. A. Bonn, W. N. Hardy, R. Liang, S. Adachi, N. E. Hussey, B. Vignolle, C. Proust, M. Sutherland, S. Krämer, J.-H. Park, D. Graf, N. Doiron-Leyraud, and L. Taillefer, *Nat. Commun.* **5**, 3280 (2014).
- [66] Y. Dagan, R. Krupke, and G. Deutscher, *Phys. Rev. B: Condens. Matter Mater. Phys.* **62**, 146 (2000).
- [67] D. T. Adroja, F. K. K. Kirschner, F. Lang, M. Smidman, A. D. Hillier, Z.-C. Wang, G.-H. Cao, G. B. G. Stenning, and S. J. Blundell, *J. Phys. Soc. Jpn.* **87**, 124705 (2018).
- [68] P. K. Biswas, Z. Salman, Q. Song, R. Peng, J. Zhang, L. Shu, D. L. Feng, T. Prokscha, and E. Morenzoni, *Phys. Rev. B Condens. Matter* **97**, 174509 (2018).
- [69] R. M. Carter, M. Casas, J. M. Getino, M. de Llano, A. Puente, H. Rubio, and D. van der Walt, *Phys. Rev. B Condens. Matter* **52**, 16149 (1995).
- [70] P. L. Richards and M. Tinkham, *Phys. Rev.* **119**, 575 (1960).
- [71] P. Townsend and J. Sutton, *Phys. Rev.* **128**, 591 (1962).
- [72] R. Escudero, E. Verdin, and F. Morales, *J. Supercond.* **7**, 381 (1994).
- [73] J. Wosnitzer, S. Wanka, J. Hagel, M. Reibelt, D. Schweitzer, and J. A. Schlueter, *Synth. Met.* **133-134**, 201 (2003).
- [74] L. P. Le, G. M. Luke, B. J. Sternlieb, W. D. Wu, Y. J. Uemura, J. W. Brill, and H. Drulis, *Physica C Supercond.* **185-189**, 2715 (1991).
- [75] T. Dvir, F. Massee, L. Attias, M. Khodas, M. Aprili, C. H. L. Quay, and H. Steinberg, *Nat. Commun.* **9**, 1 (2018).
- [76] A. P. Petrović, R. Lortz, G. Santi, C. Berthod, C. Dubois, M. Decroux, A. Demuer, A. B. Antunes, A. Paré, D. Salloum, and Others, *Phys. Rev. Lett.* **106**, 017003 (2011).
- [77] A. D. Hillier and R. Cywinski, *Appl. Magn. Reson.* **13**, 95 (1997).
- [78] W. H. Lee, S. Appl, and R. N. Shelton, *J. Low Temp. Phys.* **68**, 147 (1987).
- [79] J. A. T. Barker, R. P. Singh, A. D. Hillier, and D. M. Paul, *Phys. Rev. B Condens. Matter* **97**, 094506 (2018).
- [80] Y. J. Uemura, A. Keren, L. P. Le, G. M. Luke, B. J. Sternlieb, W. D. Wu, J. H. Brewer, R. L. Whetten, S. M. Huang, S. Lin, R. B. Kaner, F. Diederich, S. Donovan, G. Grüner, and K. Holzer, *Nature* **352**, 605 (1991).
- [81] L. Degiorgi, G. Briceno, M. S. Fuhrer, A. Zettl, and P. Wachter, *Nature* **369**, 541 (1994).
- [82] D. Varshney, R. Jain, and N. Singh, *Journal of Theoretical and Applied Physics* **6**, 25 (2012).
- [83] J. A. T. Barker, B. D. Breen, R. Hanson, A. D. Hillier, M. R. Lees, G. Balakrishnan, D. M. Paul, and R. P. Singh, *Phys. Rev. B: Condens. Matter Mater. Phys.* **98**, 104506 (2018).
- [84] D. Singh, P. K. Biswas, A. D. Hillier, R. P. Singh, and Others, *Phys. Rev. B: Condens. Matter Mater. Phys.* **101**, 144508 (2020).
- [85] D. Singh, J. A. T. Barker, A. Thamizhavel, A. D. Hillier, D. M. Paul, and R. P. Singh, *J. Phys. Condens. Matter* **30**, 075601 (2018).
- [86] J. A. T. Barker, D. Singh, A. Thamizhavel, A. D. Hillier, M. R. Lees, G. Balakrishnan, D. M. Paul, and R. P. Singh, *Phys. Rev. Lett.* **115**, 267001 (2015).
- [87] K. P. Sajilesh, D. Singh, P. K. Biswas, A. D. Hillier, and R. P. Singh, *Phys. Rev. B Condens. Matter* **98**, 214505 (2018).
- [88] D. Singh, A. D. Hillier, and R. P. Singh, *Phys. Rev. B Condens. Matter* **99**, 134509 (2019).
- [89] D. Singh, K. P. Sajilesh, S. Marik, A. D. Hillier, and R. P. Singh, *Supercond. Sci. Technol.* **30**, 125003 (2017).
- [90] D. Singh, P. K. Biswas, G. B. G. Stenning, A. D. Hillier, R. P. Singh, and Others, *Physical Review Materials* **3**, 104802 (2019).
- [91] D. Singh, S. K. P., S. Marik, A. D. Hillier, and R. P. Singh, *Phys. Rev. B Condens. Matter* **99**, 014516 (2019).
- [92] R. Movshovich, N. Kim, and D. M. Lee, *Phys. Rev. Lett.* **64**, 431 (1990).